ABSTRACT

DEPARTMENT OF PHYSICS

HARGROVE, JASMINE J. B.S. SPELMAN COLLEGE, 2011

STRUCTURAL AND ELECTRONIC PROPERTIES OF GRAPHENE-BASED MATERIALS

Committee Chair: Xiao-Qian Wang, Ph.D.

Thesis dated July 2014

This thesis includes work done on graphene-based materials, examining their unique electronic properties using first-principles density-functional calculations. Ab-initio methods such as density functional theory (DFT) are widely accepted as computational methods in condensed matter and materials physics. We begin by studying the electronics properties of graphene intercalation compounds (GICs). In order for bilayer graphene to be used for field effect transistors, the GIC must decouple the adajent graphene layers and decrease interlayer interaction. We conducted a theoretical study in order to elucidate the electronic characteristics of methane intercepted bilayer graphene under a perpendicularly applied electric field. We show that methane intercalated graphene can make a promising material for implimentations of graphene based field effect transistors since it has a controllable band gap.

Finally, we show the evolution of band structure of graphene treated with fluorinated olefins through covalent functionalization. The bonding of fluorine to the graphene surface results in the transformation of orbital hybridaztion from sp^2 to sp^3. We find that the modification of graphene's electronic properties by such a drastic change in

hybridization can lead to the elimination of the bands near the Fermi level and the opening of a band gap. We hope this work will help bring to light the promising electronic properties of graphene based materials for future device applications.

STRUCTURAL AND ELECTRONIC PROPERTIES OF GRAPHENE-BASED MATERIALS

A THESIS

SUBMITTED TO THE FACULTY OF CLARK ATLANTA UNIVERSITY

IN PARTIAL FULFILLMENT OF THE REQUIREMENTS FOR

THE DEGREE OF MASTER OF SCIENCE

BY

JASMINE J. HARGROVE

DEPARTMENT OF PHYSICS

ATLANTA, GEORGIA

JULY 2014

ACKNOWLEDGMENTS

I would first like to acknowledge the strength and power of God. I would like to thank my mother for encouraging me to follow my dreams and for believing in me always. I would like to thank my grandparents and great-grandparents for their unconditional love and support. I would like to thank my friends and extended family for always pushing me to go beyond my comfort zone and to grow in ways I never thought were possible. I would also like to express great appreciation for my advisor Dr. Xiao-Qian Wang, for without whom I could not have completed this paper. I would also like to acknowledge Dr. Natarajan Ravi for his support and advisement throughout my academic career. I would like to give a special thank you to my colleagues for their undying support, camaraderie, and wealth of knowledge. Finally, I would like to acknowledge the Department of Physics, the Department of Chemistry, and the Center for Functional Nanomaterials for their continued assistance and financial support. This work was supported NSF (Grant No. DMR-0934142).

TABLE OF CONTENTS

LIST OF FIGURES

LIST OF ABBREVIATIONS

LDA	Local Density Approximation
GGA	Generalized Gradient Approximation
DFT	Density Functional Theory
LUMO	Lowest Unoccupied Molecular Orbital
HOMO	Highest Occupied Molecular Orbital
PBE	Perdew-Burke-Ernzerhof
GICs	Graphene Intercalation Compounds
TS	Tkatchenko-Scheffler
DMol	Density functional calculations for Molecules
CBM	Conduction Band Maximum
VBM	Valence Band Maximum
PDME	perfluoro-(5-methyl-3,6-dioxanon-1-ene)
PDME-FG	perfluoro-(5-methyl-3,6-dioxanon-1-ene) functionalized graphene

CHAPTER 1

INTRODUCTION

In recent years graphene has become a popular topic in physics and material science (*1, 2*). Graphene has more publications per year than previously popular carbon allotropes such as fullerenes and nanotubes (*3*). The word graphene refers to a two-dimensional monolayer of graphite in the (0001)-plane. The hexagonal honeycomb lattice of graphene is not only found in graphite but also in carbon nanotubes and fullerenes (*4*). Therefore, graphene can be used as the basis for studying the properties of other carbon allotropes (*5*). Graphene can be used as a model for describing graphite since the distance between graphite planes (3.37 Å) is larger than the distance between carbon atoms in the same plane (1.42 Å). The intralayer bonds are much stronger than the interlayer bonds (*6, 7*).

The two equivalent triangular sublattices A and B in graphene result in a band structure that has a linear energy dispersion relation for electrons in which the energy is proportional to the crystal momentum (*7*). Figure 1.1 shows the graphene band structure near the Dirac point. Since the conduction band and the valence band intersect at the Dirac point, graphene is classified as a zero band gap material as shown in Figure 1.2. Graphene is unique because the Hamiltonian is equal to the relativistic Dirac equation with zero effective mass in the low energy spectrum. The electrons in graphene are called

massless Dirac fermions because the Fermi velocity of the electrons is a fraction of the speed of light *c(7)*. Although the relativistic Dirac equation the wave function is a two-component vector which comes from the two spin angular momentum components (+1/2 and -1/2). The wave function for electrons in graphene have two components that come from the sublattices A and B. A and B are also known as psuedospin components.

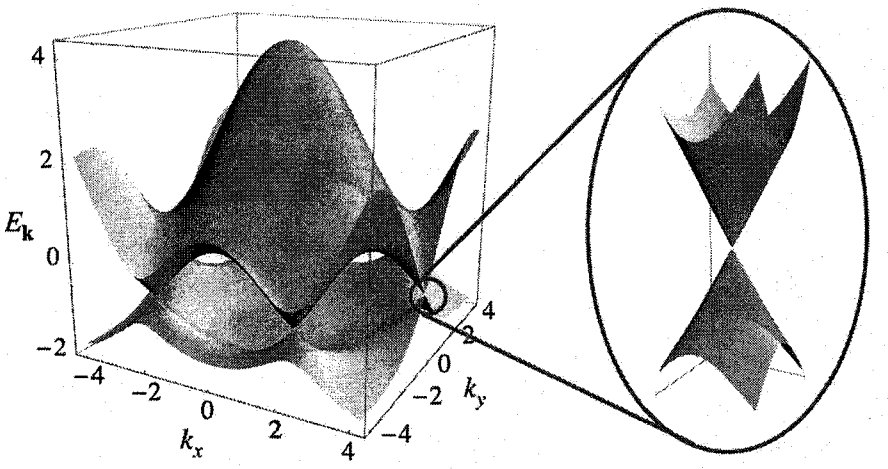

Figure 1.1. Band structure of graphene. The energy of the conduction band and the valence band as a function of wavevector k.

The wave function near the Dirac point is chiral and this leads to various unique features of graphene such as half-integer quantum Hall effects, Klein tunneling and universal quantum limited conductivity (*8,9*). As a consequence of graphene's unique band structure, the electrons in graphene act like massless Dirac fermions that have a Fermi velocity that is ten times higher than silicon (*7*). Also, the carriers in graphene can travel up to 400nm at room temperature without any scattering. Therefore, graphene is characterized by very high mobility. Recent studies have shown that the mobility of

suspended graphene devices can be up to 1,000,000 cm^2/Vs. The hole mobilities in graphene are also much higher than in any other semiconductor (*10*). However, the channel mobility in graphene can be degraded somewhat by edge roughness and top-gate fabrication.

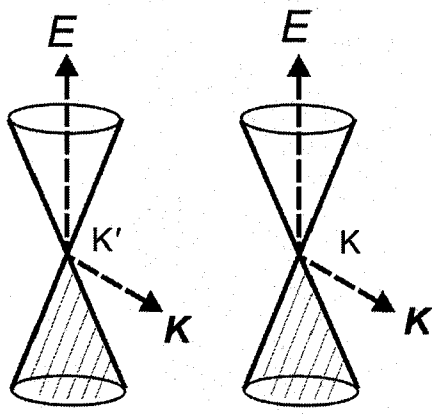

Figure 1.2. Energy dispersion near the Dirac points (K, K').

Graphene has the ability to avoid short-channel effects when the channel length is scaled down since it is a two-dimensional material with one atom layer thickness (*11*). In the semiconductor industry, it is desirable to increase the speed of operation and the number of components per chip by restricting the channel length. Although, limiting the gate length in a material can lead to several short channel effects such as drain-induced barrier lowering (DIBL), threshold voltage roll off, and even poor sub-threshold slope, two-dimensional structure of graphene allows it to be scaled down without significant short channel effects (*12*). High-field transport properties are also important when considering channel length in graphene systems. Graphene field effect transistors can achieve carrier velocities much faster than silicon. Therefore, graphene can be used to create higher speed transistors.

Graphene field emissions transistors have a low on/off ratio that causes an off-state leakage which makes pure graphene undesirable for logic circuit applications. There are two reasons for the poor switching ability of graphene, the first being that large area graphene has zero band gap. Graphene does not have the quadratic relation found in most semiconductors but instead the energy momentum relation is linear for electrons in the conduction band. Band gaps can be induced in the graphene systems by external electric fields and chemical doping. Secondly, Klein tunneling that occurs in graphene systems also affects its ability to be used for logic circuit applications. In quantum mechanics, particle tunneling occurs when energetic particles are transmitted through a potential barrier which has a height that is higher than its kinetic energy. The transmission probability of non-relativistic particles depends on the height and width of the energy barrier (*9, 13*). It is difficult to switch graphene off completely because, the electrons can tunnel through very high and sharp energy barriers. Nevertheless various doping techniques have been investigated in order to use graphene as a transistor. These unique properties of graphene systems have led to increased interest in these materials.

As graphene has become the basis for studying relativistic condensed matter physics, various approaches to the fabrication of graphene have emerged. Novoselov produced exfoliated graphene by peeling it off of a graphite crystal with tape (*14*). Epitaxial graphene is grown on a substrate which gives rise to unique interactions. Some of the interactions that have been observed are a blueshifted Raman Spectrum and a shift in the Dirac point below the Fermi level due to doping (*14-17*).

The unit cell of graphene contains two nonequivalent atoms, A and B as shown in Figure 1.3. Each of the atoms has four valence electrons. Three out of the four electrons form σ covalent bonds at high binding energy, which gives graphene a very strong structural rigidity. The fourth electron is in a delocalized π orbital which crosses the Fermi energy at the Brillouin zone. The Brillouin zone is located in the reciprocal space of graphene. a1 and a2 are the lattice vectors, where a is the lattice constant a=2.46 Å. In 1947, Philip Wallace utilized the nearest neighbor tight-binding model on the hexagonal crystal lattice and developed the first tight-binding description of graphene (18). Wallace ignored the overlap between the wave functions from more remote atoms.

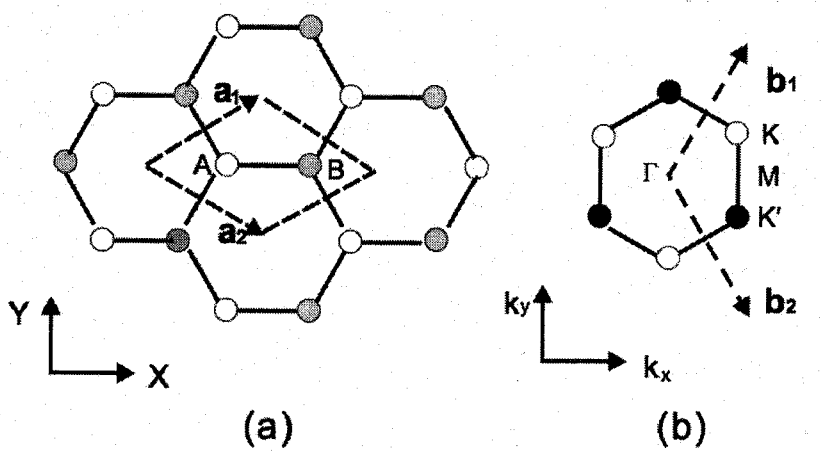

Figure 1.3. Graphene hexagonal lattice and first Brillouin zone. (a) Graphene hexagonal lattice. a_1 and a_2 are the lattice vectors. (b) Sketch of the first Brillouin zone in the reciprocal lattice.

The thesis is organized as follows: Chapter 1 is an introduction of graphene. Chapter 2 describes the theory behind the method used in the calculations. Chapter 3 discusses results of a theoretical calculation of the structural and electronic characteristics of methane intercalated graphene. Chapter 4 discusses the chemical functionalized

graphene through a [2+2] cycloaddition mechanism. Finally, Chapter 5 presents conclusions and future work. The research reported in this thesis has resulted in one journal publication entitled Band gap opening in methane intercalated graphene, which was published in Nanoscale (*19*).

CHAPTER 2

DENSITY FUNCTIONAL THEORY

Molecular modeling is used in order to better understand materials of interest. Although computational models can be used, they must be based on quantum mechanical laws that allow one to determine the exact electronic structure of atoms. Electrons tend to couple which leads to problems finding a solution for systems containing more than one electron. The complexity of finding an analytical solution increases drastically as the number of electrons increases. Solving Schrödinger's equation allows for the properties of a time-dependent non-relativistic system to be determined (*20*). The Schrödinger equation also serves as the foundation of Density Functional Theory. The Schrödinger equation with the Hamiltonian operator is difficult to solve without simplifying the Hamiltonian.

Born and Oppenheimer were able to find a way to simplify the Hamiltonian with the Born-Oppenheimer approximation which states that the motion of the nuclei is slow compared to the electrons since there is a three magnitude difference between mass of the nuclei and electrons. Because the many-electron wave function contains 3N variables, the Schrödinger equation can not be solved by the previously mentioned Hamiltonian since it is too complex. Other methods of finding approximations for this many-body problem must be employed. Two methods that can be used are the Thomas-Fermi theory and the Hartree-Fock theory.

Thomas and Fermi proposed a unique approach to solving the many-body problem. Instead of using the many-body wave function, Thomas and Fermi proposed the electron density to be used as the central variable and the total energy of the system to be a functional of the density (*21, 22*). Although the Thomas-Fermi method has been used in the past due to its ability to give a good approximation of the charge density and electrostatic potential, it does have its drawbacks. A key deficiency in the Thomas-Fermi method is that at the nucleus the charge density is infinite but does not decay exponentially from nucleus as expected. The approximation used for the kinetic energy, can also cause errors in results. Once the Thomas-Fermi method is employed, the output never results with atoms forming solids or molecules (*23-25*). Another issue with the Thomas-Fermi method is that the electron-electron interactions are treated classically and don't take into account vital quantum mechanical phenomena (*26*).

The Hartree-Fock theory, which was proposed by Hartree and Fock, is based on a single-particle approximation. Hartree added an addition exchange interaction between the electrons by using antisymmetric single-particle functions. Hartree was able to expand the wave function of many electrons into a single electron wave function. The Hartree approximation does not account for any exchange interactions. The Pauli Exclusion Principle caused the Hartree approximation to fail because the wave function is not antisymmetric. This issue was solved by the Hartree-Fock approximation which allowed the wavefunction to be written as antisymmetrised product of orbitals (*27*). Electrons are fermions and their wave function must be antisymmetric. The Slater determinant can be used to evaluate the approximation of the wave function. The Hartree-

Fock energy can be found by evaluating the expectation value of the Hamiltonian with the Slater determinant. The Hartree-Fock method is a considerable improvement over the Hartree theory since the many-electron wave function is formed from antisymmetric single-electron wavefucntions. The Hartree-Fock method is most suitable for materials with a small number of localized electrons such as oxides or crystals of small organic molecules. The Hartree-Fock method is not useful for pure metal systems since it ignores coulombic interactions among electrons that are not localized (*28*).

Hohenberg-Kohn Theorems are the fundamental building blocks of modern Density Functional Theory. The theorems were first proposed in 1964 (*29*). Walter Kohn received the Nobel Prize for his contribution to the development of DFT in 1998. DFT has been one of the most used ab-initio methods in solid-state physics due to it being fast, accurate and suitable for large systems such as crystals and surfaces (*30*). The Thomas-Fermi and Hartree-Fock methods are considered predecessors of DFT. DFT is based on the electronic charge density distribution n(r) and is exact for the ground state (*31*).

Density Functional Theory provides a simple method for modeling the effect of exchange and correlation in an electron gas. DFT is able to deal with systems that are inhomogenous but have identical particles (*32*). Kohn and Sham were able to show that the many-electron problem can be substituted by an equivalent set of one-electron equations (*33*). In 1965, Kohn and Sham showed that the Hamiltonian equations derived from this variation approach have a simple form that is similar to the time-independent Schrödinger equation (*33*).

Density Functional Theory has many applications in various fields such as geophysics, biomaterials, and nanomaterials (*34*). DFT has been used for degenerate ground states, magnetic and electric susceptibilities, and even quantum Hall effects (*35*). Although DFT has many applications, there are some failures of DFT which include not taking into account van der Waals interactions, underestimated band gaps by Local Density Approximation (LDA) and General Gradient Approximation (GGA), and larger binding energies for Local Density Approximation.

The exchange-correlation potential is a functional derivative of the exchange correlation energy. This exchange correlation energy is with respect to the local density. For a homogenous electron gas, the local density only depends on the density of the electron gas. In nonhomogeneous systems, the exchange correlation depends not only on the density at a certain location but also on various locals close to this location (*36*). Local Density Approximation is the easiest way to describe the exchange-correlation energy of an electronic system (*33*). LDA is made by assuming that the exchange-correlation energy per electron in a homogenous electron gas has the same density as an electron some distance away. In this approximation is it assumed that there is an exact density at each point in a specific region. Each of these points have the same many-body response by the surrounding electrons. The exchange-correlation energy can be integrated over the entire volume element. Although LDA works well for many systems with valence charge density that varies slightly, it is much less accurate for systems with chemical bonds. Another assumption made by LDA is that the exchange-correlation energy functional is local. The parameterization that exists for the exchange-correlation

energy of homogeneous electron gas has similar results in terms of energy (*33*, *37-38*). The Local Density Approximation can be used to predict electron densities, atomic positions, and vibration frequencies among others (*39*). Density Functional Theory can provide robust predictions for the electronic structure of various material systems and verify experimental results.

CHAPTER 3

METHANE INTERCALATED BILAYER GRAPHENE

3.1 Introduction

For the last 40 years band gaps have been a topic of discussion in scientific research. Since graphene is a material with zero band gap, the task has then become to create a band gap within graphene. A great deal of interest has been generated by the idea of inducing a band gap by the use of graphene intercalation compounds otherwise known as GICs. Recent experimental advances have demonstrated GICs that are formed by insertion of molecular layers with various chemical species between graphene layers (*40*). The choice of intercalant species and amount of intercalation provides a novel way to control various properties like carrier concentration and interlayer electrical conductivity. Moreover, GICs that can induce a band gap in graphene are also being considered for energy storage, nanoelectronics, and spintronics (*41-43*). A variety of potential applications using different intercalants, such as hydrogen, metal clusters, and methane, have been examined (*44-49*). Few-layer graphene systems can affect the band structure in various ways. There have been numerous studies of calculated low energy band structures of few-layer graphene systems, such as bilayer (*AB* or *AA* stacked), trilayer (*ABA* or *ABC* stacked) and tetralayer (*ABAB*, *ABCA*, *ABAC*, and *ABCB* stacked) (*50-53*). It has been shown that *AB* bilayer graphene without an external electric

field applied is a zero gap semimetal with a parabolic dispersion. Once a perpendicular field is applied, the two graphene layers are no longer equivalent. However in *ABA*-trilayer graphene, which is a semimetallic system in which there is a slight overlap between the conduction and valence bands, a band gap is not induced when an external electric field is applied. *ABC*-trilayer graphene is a zero-gap semiconductor with a band contact near the K-point on the KM symmetry line and opens a band gap at the K-point under an electric field. Starting from tetralayers graphene systems, band gaps are not created by an external electric field and are all semi-metallic at zero field (*50*, *51*). In this chapter, the effects of methane as an intercalated compound for *AB* and *AA*-stacked graphene with and without an externally applied electrical field are investigated.

3.2 Methods

The first step in determining the effects of methane on the band gap of graphene is investigating the structural and electronic properties using Density Functional Theory. For the exchange-correlation the General Gradient Approximation was used with Perdew Burke Ernzerhof (PBE) parameratization which is a theoretical method used to investigate the electronic state particularly with an interest in the ground state of molecular bodied systems. With the use of the Tkatchenko-Scheffler (TS) scheme, dispersion correction accounts for the some of the inaccuracies in the computation of the band structure of the molecular body of interest.

In order for one to grasp a full understanding of the electronic properties of methane intercalating graphene, one must understand and appreciate the band structure of methane. Although, DFT is a completely systemic approach which has proven to be

rather useful it does not allow one to examine van der Waals interactions. Therefore we employed the PBE parametrization followed by the TS scheme. The importance of the TS scheme is to determine the relationship between volume and polarizability. In this theoretical model, bilayer graphene with a 2 x 2 cell was intercepted with a methane molecule. The bilayer systems serves as the hallmark model of the methane intercepted graphene. A 6 x 6 x 1 super cell with a vacuum space of 16 Å normal to bi-layer graphene system was used. The Monkhorst-Pack K-point grids of 6 x 6 x 1 were used since they are foundational for the determination of the lattice. The geometry optimization convergence criterion was satisfied when the kinetic energy change was approximately 3×10^{-4} eV which was influenced by the charge density of the system.

Figure 3.1 shows two layers of graphene deeply intercalated with methane. On the left there is the AA graphene and on the right there is the AB graphene with the intercalated methane component. In order to model the methane in bilayer graphene, a 2 x 2 cell of bilayer graphene intercalated with a methane molecule was used. Evaluating the symmetry of AA and AB-stacked bilayer graphene, there is an odd as well as an even symmetry in what one would call the sublattice exchange. The Bernal-stacked pattern which is known as the AB-stacked can be grown on the C-face (000-) of the SiC substrate. In direct comparison, the AA stacking has carbon atoms positioned in the first layer aligned with carbon atoms of the next layer. A Dirac fermion behavior will manifest itself when the methane is successfully intercalated within the graphene structure. It was determined that the C-face multilayer graphene is not AB stacking but in fact its atoms

are non-symmetrical stacked. Bilayer graphene is analogous to a composite of isolated graphene sheets or quasi-free-standing graphene.

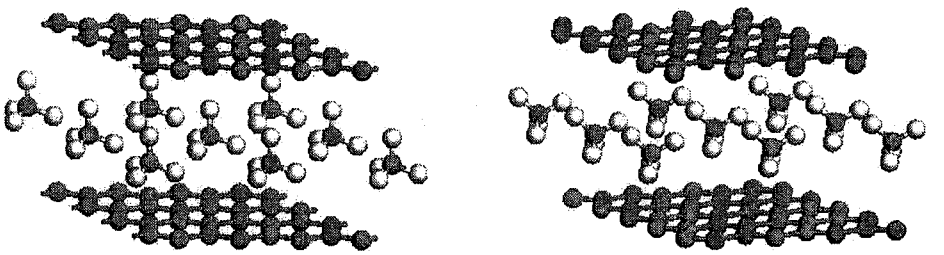

Figure 3.1 Perspective view of optimized structures of two layers of graphene. The *AA* and *AB*-stacked graphene layers sandwiched with methane are shown in the left and right panels, respectively.

When examining the *AA*-stacked bilayer graphene , linear dispersion bands appear. This sublattice exchange is an even symmetry in which the interlayer electronic coupling is down regulated by the Pauli repulsion between the two graphene layers. This sublattice has a great impact on the electronic band structure. The *AB*-stacked bilayer displays a parabolic dispersion and is semi-metallic due to the given Fermi levels.

The intercalated methane molecule in the *AA*-stacked bilayer has approximately three hydrogen atoms which are directed at the lower level of the graphene layer which also forms in a parallel fashion. There is a forth hydrogen atom that does not point in the similar direction. The forth is theorized to point straight up towards the top layer of graphene. The planar hydrogen atoms maintained the C_{3v} symmetry of the methane intercepted graphene bilayer. From the DFT calculations, it was shown that the *AA* stacking is slightly lower than the *AB* stacking in terms of energy. There was an absence of distortion of methane found after intercalation; thus this was seen in the carbon to

hydrogen distance at 0.96 and 0.98 Å for *AA* and *AB*-stacking respectively. The tetrahedral angle is 109.66° and 109.51° in respect to *AA* and *AB* stacking. There was also expansion found between the layers being 6.994 and 6.992 Å for both *AA* and *AB* stacking. With a low significant difference of 0.003 Å, it is expected that the layers are relatively flat.

3.3 Results and Discussion

The *AB* and *AA* stacking systems have the energy differences -0.031 and -0.153 eV per carbon atom, respectively. The significant increase in stability of *AB*-stacked bilayer with methane intercalation compared to *AA*-stacked is because of its unique methane interception conformations. Despite the methane intercalation decreasing the interlayer coupling, the methane influenced interactions are vital in developing optimal intercalated conformations.

AB bilayer graphene intercalated with methane exhibits a clear gap at the Dirac point due to interlayer coupling. After the bilayer graphene system is intercepted with methane, the exceptional band structure characteristics related to sublattice exchange symmetry are inactive. The *AA* and *AB*-stacked conformations exhibit similar band structures. The π and π^* bands for methane intercalated structures that once formed Dirac cones are now pulled apart which is likely suggestive of quasi-free-standing graphene.

We illustrate in Figure 3.2 the corresponding *AA* and *AB*-stacked band structures. As seen in Figure 3.2, the band structure of *AA*-stacked bilayer graphene shows two Dirac crossings in the proximity of the K-point. In contrast, the *AB*-stacked bilayer displays two parabolic bands with a separation of 0.37 and 0.43 eV for conduction and valence bands,

respectively (*54*). Since our results are in agreement with the experimental findings that the methane intercalated graphene provides an innovative approach for systems displaying free-standing monolayer graphene behavior, it is imperative to explore the ability to engineer a band gap for electronic transistor devices (*44*, *55-69*). Therefore, investigating methane intercalated bilayer graphene under a perpendicularly applied electric field is important.

Figure 3.2 (c) and (f) represent the band structure for AA and AB-stacked bilayer with an electric bias, respectively. Once electric bias is applied, the electronic states near the Fermi level go back to the corresponding AA and AB-stacked characteristics in the absence of the methane intercalation which can be attributed to the enhanced dipole interactions as a result of applying electric bias (70). The AA-stacked band structure is analogous to AA bilayer with methane intercalation and electric bias tuning the "distance" of the doubled Dirac crossing (70). For methane intercalated AB-stacked with electric bias, the widest gap was induced. Whether or not there is a gap opening depends on constraints associated with the sublattice exchange (70, 71), as the AA and AB stacking yields distinctive responses to the electric bias (70, 71). For the AA-stacked graphene system, the single Dirac cone splits into two Dirac cones and the separation of the two cones in the momentum space is proportional to the applied electric bias (70). However, the methane-intercalated, AB-stacked bilayer graphene has a tunable gap as a result of an applied electric bias.

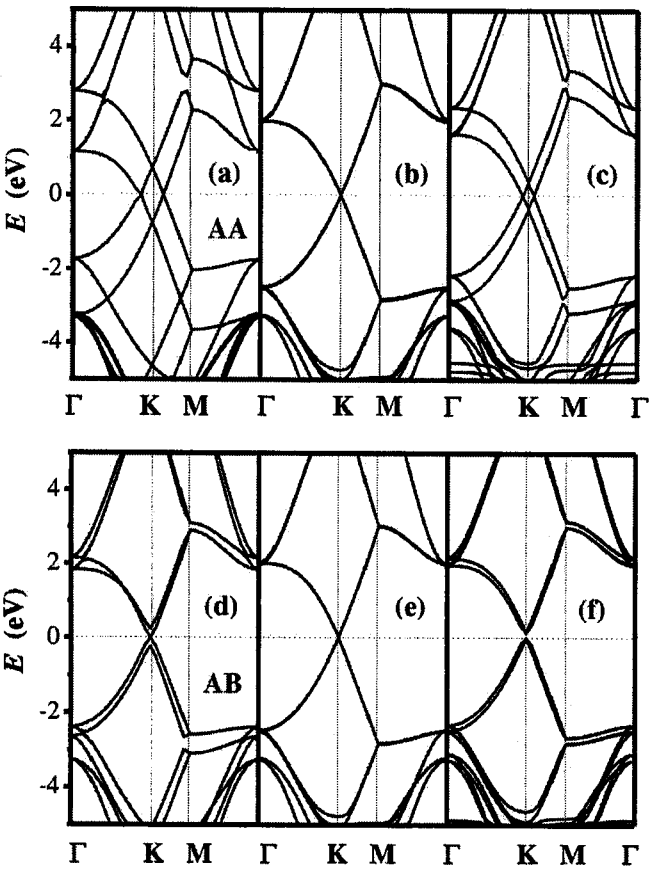

Figure 3.2 Calculated band structure of bilayer graphene. (a), (b), (c) for *AA*-stacked bilayer and (d), (e), (f) for *AB*-stacked bilayer, without intercalation (left panels), with methane intercalation (middle panels), and methane-intercalated graphene with 0.26 V/Å electric bias (right panels), respectively. $\Gamma = (0, 0)\ \pi/a$, $K = (-\pi/3a, 2\pi/3a)$, $M = (0, \pi/2a)$, where a = 4.887 Å. The Fermi level, highlighted by dashed red line, is shifted to 0 eV.

Figure 3.3 shows the extracted band gap versus the variation of electric bias. As seen in Figure 3.3, the methane intercalated *AB*-stacked bilayer graphene shows a tunable gap with the application of the electric bias. The largest value of the gap is about 0.32 eV at an electric field of $\varepsilon = 0.15$ V/Å. Figure 3.3 exhibits the extracted electronic charge density of near gap states. Figure 3.3 also demonstrates that the electronic wave functions at zero bias follows a chain feature for the π and π^* states. The electric bias

caused the charge in the *AB*-stacked bilayer graphene to be isolated and is related to the breaking of the sublattice symmetry, which is a prerequisite for the gap opening (*70-72*).

In GIC systems, it is expected to have both *AA* and *AB*-stacked regions as twisted bilayers, which are the principal stacking pattern for multilayer graphene (*73*, *74*). The methane-intercalated AB-stacked bilayer graphene is an ideal candidate for electric field induced band gap opening. The electric bias induced dipole-dipole interactions caused a gap opening in the AB-stacked bilayer system. As a result, there was also charge transfer

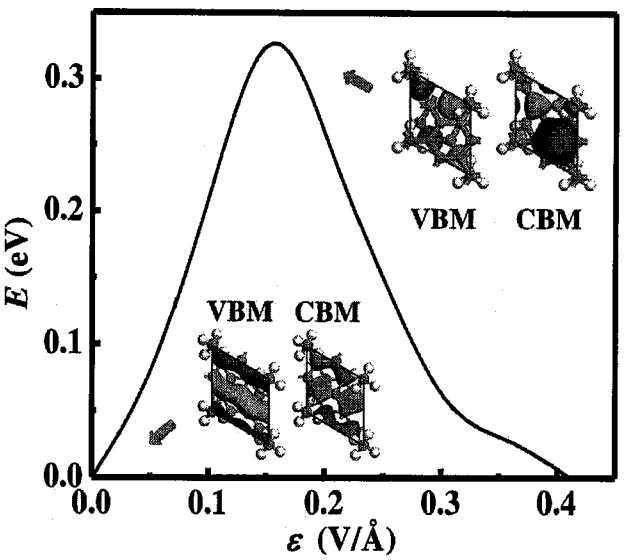

Figure 3.3 Calculated dependence of the energy gap on the applied electric bias for *AB*-stacked methane-intercalated graphene. Insets: extracted charge density of valence band maximum (VBM) and conduction band minimum (CBM) at the band center, with different wave function components colored with blue and yellow, respectively.

between the conduction and valence states due to dipole-dipole interactions (*62-67*). On the contrary, further increase of the electric bias reduces the band gap because of the level hybridization of other near gap states. The linear dispersion near the Fermi level

remained even after the opening of a band gap (*66-69*). This feature is essential for both fundamental device applications and the transport of charge carriers. Also, the dispersion correction is necessary for an accurate description of the 85 structural and electronic properties. Our current approach based on dispersion-corrected DFT provides quantitatively accurate results for the layer distance which are found to be 3.512 and 3.412 Å for *AA* and *AB*-stacked bilayer, respectively which are improved results over the lack of dispersion correction (*70*). Moreover, a modified Hamiltonian for electronic structures includes the effect of electric bias (*70*).

3.4 Conclusion

In summary, the evolution of electronic properties of methane-intercalated graphene as a function of the applied electric bias has been studied using theoretical dispersion corrected DFT calculations. The present work demonstrates that significant control of the low energy electronic states of graphene can be accomplished by tuning interlayer interactions through methane intercalation. The additional control of the electronic properties of intercalated graphene as a function of electric bias should extend the range of distinctive physical phenomena and applications for nanodevices. We remark, before closing, that the interlayer coupling plays an important role in a variety of graphene based systems, which is considered as a promising substrate for device applications. We hope that the prediction of a band gap opening that is tunable by the electric bias can be used to promote further experimental investigation in methane intercalated graphene materials.

CHAPTER 4

CYCLOADDITION OF GRAPHENE

4.1 Introduction

Graphene, a two dimensional material with massless fermions, has unique electronic properties, due to its peculiar electron energy spectrum. It is a unique crystalline material with a linear dispersion law, making its electron mass virtually approach zero. As a result, graphene has remarkably high electron mobility, which positions it as a potential material for future fabrication of micro- and nanoelectronic devices. However, the absence of a band gap is a major downside for graphene. However, graphene may still be able to be used in microchips of electronic and optoelectronic devices if it can be made semiconducting by functionalization, the explicit covalent bonding of molecules to its surface (*75*, *76*).

Recent experimental work has focused on the idea that covalently functionalized graphene will produce a change in its electronic properties depending on the number and the type of absorbed molecules. As shown in Figure 4.1, pure graphene is a sp^2-hybridized carbon network in two dimensions, with a zero bandgap (*77*). Each carbon atom has six electrons. Two of the carbon electrons are core electron. They are bound tightly to the nucleus and do not participate in binding with neighboring carbon atoms. The other four electrons are valence electrons. Two of them sit in 2s states, while two of

them occupy 2p states. When carbon atoms are bonded together to form graphene, the two 2s orbitals and two 2p orbitals interact with each other to form three in-plane covalent bonds (σ bonds) through sp^2 hybridization (*78*). Each atom has three nearest neighbors. The σ bonds are strong and contribute to graphene's exceptional mechanical performance. A delocalized electronic state (π bond) is formed perpendicular to the graphene plane, which contributes to its special transport properties. When carbon atoms in graphene interact with other chemical species, their electronic bonding structures can be modified. There are two types of surface functionalization: covalent and non-covalent bonding (*79*). In covalent functionalization, carbon atoms form covalent bonds with other

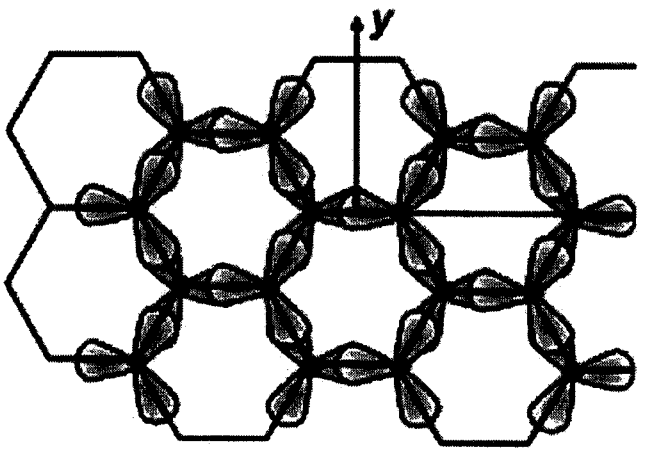

Figure 4.1. Schematic of bonds between neighboring carbon atoms in graphene.

chemical species. In non-covalent functionalization, carbon atoms form van der Waals bonds with the functioning chemical species. When covalent functionalization occurs, sp^2 hybridization will change into sp^3 configurations (*79*). In fact, if one exposes graphene to hydrogen plasma, hydrogen atoms will form covalent bonds with graphene and position themselves on alternate sides of adjacent carbon atoms (*80*). Fully hydrogenated graphene is called graphane.

The hybridization state of carbon atoms from sp^2 into sp^3 is that a band gap results in the highly conductive graphene (*80*). It is theoretically calculated that the band gap of graphane can reach up to 5.4 eV (*81*). Moreover, recent work has shown that hydrogenated graphene is reversible and its electronic properties could be tuned by controlling hydrogen adsorption (*80*). Given the very large band of hydrogenated graphene (graphane) and the zero band gap of graphene, it may be possible to engineer the band gap over a wide range by tuning the hydrogen treatment (*82*). Fluorine is also exciting for a variety of applications due to its functionality as increasing hydrophobicity, reducing surface energy, and its usefulness in bio-applications (*83-84*). However, hydrogen and fluorine can be damaging to graphene and decrease its carrier mobility. Chlorine can also be used to functionalize graphene. Theoretical work has shown that by exposing both sides of graphene to chlorine the band gap can be opened up to 1.3 eV (*85*). Chemical functionalization of graphene, particularly by hydrogen, fluorine and chlorine, has shown interesting results, such as doping, edge passivation and widening of the band gap of the resulting material (*86-87*). However, how to functionalize graphene and characterize it is still a challenge.

The primary issue in any functionalization is whether a functionalizing molecule acts as an electron donor, or as an electron acceptor. The charge of a molecule bound to a graphene sheet is increased or decreased compared to the molecule in free state. To date, most of the electrical conductance work has been focused on carbon nanotubes (*88*). As stated before, the purpose for functionalization is to induce a band gap in graphene. Recent experimental work have demonstrated that cycloaddition of fluorinated olefins

represents an effective approach to reduce the off currents of mixed nanotube mats for transistor applications. We have studied the electronic structure characteristics of the corresponding [2 + 2] cycloaddition using dispersion-corrected density functional calculations. The band gap opening in chemically functionalized graphene is associated with the sp^2 to sp^3 rehybridization. Our calculation shows that the experimentally observed suppression of semimetallic conductivity can be attributed to a symmetry aligned cycloaddition scheme that transforms semimetallic graphene to semiconducting. Despite the exciting experimental findings, the mechanism of the exclusive conversion remains unclear. Specifically, it was suggested that the change from semimetallic to semiconducting behavior can be induced either through scattering centers associated with the covalent functionalization or through band structure modifications (*89*). In order to facilitate an in depth understanding of this mechanism, we have performed calculations based on DFT. The cycloaddition of olefins involves an unusual thermally allowed [2 + 2] cycloaddition. Specifically, the highest occupied molecular orbital (HOMO) of the olefin, π, intersects with the conduction band of the graphene, while the lowest unoccupied molecular level (LUMO) of the olefin, π^*, interacts with the valence band of graphene. Our findings demonstrate the nature of the [2 + 2] cycloaddition of perfluoro-(5-methyl-3,6-dioxanon-1-ene) (PMDE) with graphene.

4.2 Method

The structural and electronic properties and optimization of geometry was calculated within the framework of the Density Functional Theory as implemented in the DMol3 package. Dispersion- and gradient-corrected PBE was used (*74*). The LDA approach is

suitable for weakly interacting π systems while dispersion-corrected GGA provides a more accurate description. Geometry optimization convergence criterion was satisfied when the total energy change was less than of 3 $x10^{-5}$ eV. The Generalized Gradient Approximation in exchange–correlation parameterization was used for band structure calculation. For the band structure computation the selected K- path was Γ–M–K-Γ. Although the GGA approach systematically underestimates the band gaps, we were primarily interested in the mechanism of band gap opening. For that purpose the GGA approach was expected to provide qualitatively correct information. Periodic-boundary conditions were employed with a supercell in the *xy* plane large enough to eliminate the interaction between neighboring replicas. A double numerical basis was sufficient for the grid integration of the charge density to converge. All structures were relaxed with forces less than 0.01 eV/Å.

4.3 Results and Discussion

We illustrate in Figure 4.2 the two optimized structures of PMDE functionalized graphene formed by [2+2] cycloaddition. Figure 4.2 (a) shows PDME adduct attached to 3^{rd} and 4^{th} carbon. Likewise, Figure 4.2 (b) shows the PDME adduct attached to the 2^{nd} and 3^{rd} carbon. The adduct has distorted the graphene surface in both configuration by lifting the two carbon atoms attached to it above the other atoms in the graphene lattice. The adduct has increased in the bond lengths connecting the atoms on graphene to 1.50 Å. The length of the C-C bonds within the four-membered ring is ~1.59 Å for both PDME orientations.

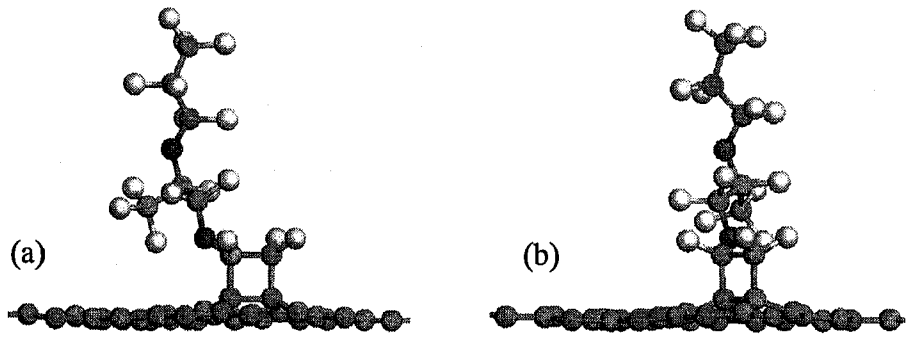

Figure 4.2. Perspective view of optimized structures of PDME functionalized graphene.

The extracted band structures in Figure 4.3. It can be seen that the widest gap that can be induced in graphene by functionalization with a single PDME functionalization is 0.28 eV for both models. This is more than 100 times higher than the thermal energy at room temperature and thus can find commercial application in the microelectronic industry, providing a feasible on/off ratio for transistors.

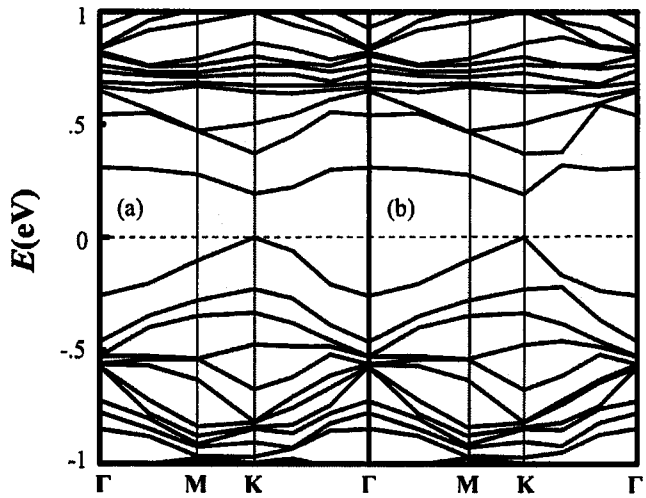

Figure 4.3. Calculated band structure of PDME functionalized graphene. (a) Band structure of graphene with PDME adduct attached to graphene (b) Band structure of graphene with PDME adduct in alternate orientation to graphene

Band structure of perfluoro-(5-methyl-3,6-dioxanon-1-ene) functionalized

graphene (PDME-FG) resembles that of graphene, as shown in Figure 4.3. Previously intersecting π and π^* bands that formed the Dirac cones are now pulled apart by the underlying σ bands, arising from the interaction of the heteroatom with the system of graphene's p_z orbitals. This σ–π interaction causes rehybridization of the carbon atoms from the sp^2 to sp^3 state. The degree of additional hybridization is directly related to the band gap. The energy similarities between the two distinct conformations is quantum in nature, as it is correlated to the degree of changes of the π network.

4.4 Conclusion

In summary, the stability of a [2 + 2] reaction of the PMDE olefin on graphene was calculated. The addition of olefins to the semi-metallic surface of graphene leading to band gap formation is related to the quasi-bound states within the energy gap that originate from the olefin (*89*). The formation of these states is particular to divalent additions, in contrast to monovalent functionalizations where localized states are formed (*90*). Our results further delineate the essential difference between semi-metallic and semiconducting graphene. Band structure analysis is imperative in order to study covalent interactions between molecules and graphene because of the associated quantum effect. Our result indicate that scattering centers play little role in the conversion of the semi-semi-metallic features to semiconducting ones, since π network disruption features associated with flat bands are not observed in our calculations. The key result is that the symmetry allowing [2 + 2] always exists for semi-metallic graphene, albeit not necessarily at the band center. Furthermore, we note that dispersion-corrected approximations are better suited to study these functionalized systems, as evidently

demonstrated by the improved binding of dispersion-corrected GGA results over the LDA ones. These results shed light on the preferential [2 + 2] cycloaddition of olefins to the semi-metallic graphene relative to the semi-metallic and semiconducting ones.

CHAPTER 5

CONCLUSION AND FUTURE WORK

The methane intercaltion and functionalization resulted in an induced band gap when subjected to electric bias have been presented. Specifically, a tunable band gap induced due to methane intercalated *AB*-stacked bilayer system exposed to an electric bias. The [2+2] cycloaddition of olefin with graphene resulted in an induced band gap for two adduct-graphene conformations.

It is worth noting that the DFT approach can be used for many systems including nanostructures such as carbon nanotubes and nanoribbons. In the future, further invetigation on various chemical species differing from those discussed in this thesis will be investigated. Studying the effects of electric bias and band gap tunability on a vast range of multilayered and chemically doped graphene systems will improve our understanding of the mechanisms by which these configurations affect electronic structures. Cycloaddition and intercalation of graphene with atoms and molecules that may be relevant will be invesiagted. Experimentally validating calculated results based on theory will be useful in order to test the accuaracy of our predictions.

REFERENCES

[1] Geim, K. Graphene: Status and Prospects. *Science*, **2009**, 324, 1530–1534.

[2] Neto, A. H. C.; Guinea, F.; Peres, N. M. R., K.; Novoselov, S. and Geim, A. K. The electronic properties of graphene. *Reviews of Modern Physics*, **2009**, 81, 109–161.

[3] Barth, A. and Marx, W. Graphene - a rising star in view of scientometrics. *Tech. Rep.*, **2008**, 1, 118.

[4] Saito, R.; Dresselhuas, G. and Dresselhaus, M. S. *Physical properties of carbon nanotubes*. World Scientific Publishing Company, 1998.

[5] Wallace, P. R. The band theory of graphite. *Phys. Rev.*, **1947**, 71, 622–634.

[6] Painter, G. S. and Ellis, D. E. Electronic band structure and optical properties of graphite from a variational approach. *Phys. Rev. B*, **1970**, 1, 4747–4752.

[7] Geim, A. K. and Novoselov, K. S. The rise of graphene, *Nature Materials*, **2007**, 6, 183-191.

[8] Abergel, D. S. L.; Apalkov, V.; Berashevich, J.; Ziegler, K.; and Chakraborty, T. Properties of Graphene: A Theoretical Perspective," *Advances in Physics*, 2010, 1-17.

[9] Allen, M. J.; Tung, V. C. and Kaner R. B. Honeycomb Carbon: A Review of Graphene. *Chem. Rev.*, **2010**, 110, 132-145.

[10] Dorgan, V. E.; Bae, M.-H.; and Pop, E. Mobility and saturation velocity in graphene on Si02. *Applied Physics Letters*, 2010, 97, 082112-082112-3.

[11] Schwierz, F. Graphene transistors. *Nature Nanotechnology*, 2010, 5, 487-496.

[12] Taur. Y. and Ning, T. H. *Fundamentals of Modern VLSI Devices.* Cambridge University Press, 2009.

[13] Katsnelson, M. I.; Novoselov, K. S. and Geim, A. K. Chiral tunneling and the Klein paradox in grapheme. *Nat. Phys.*, **2006**, 2, 620-625.

[14] Novoselov, K. S.; Geim, A. K.; Morozov, S. V.; Jiang, D.; Zhang, Y.; Dubonos, S. V.; Grigorieva, I. V. and Firsov, A. A. Electric Field Effect in Atomically Thin Carbon Films. *Science*, **2004**, 306, 666-669.

[15] Lee, D. S.; Riedl, C.; Krauss, B.; von Klitzing, K.; Starke, U.; and Smet, J. H. Raman spectra of epitaxial graphene on SiC and of epitaxial graphene transferred to SiO2. *Nano Lett.*, **2008**, 8, 4320-4325.

[16] Ferralis, N.; Maboudian, R. and Carraro, C. Evidence of structural strain in epitaxial graphene layers on 6H-SiC(0001). *Phys. Rev. Lett.*, **2008**, 101, 156801.

[17] Seyller, T.; Bostwick, A.; Emtsev, K. V.; Horn, K.; Ley, L.; Mcchesney, J. L.; Ohta, T.; Riley, J. D.; Rotenberg, E. and Speck, F.. Epitaxial graphene: a new material. *Physica status solidi*, **2008**, 245, 1436-1446.

[18] van Schaijk, R. T. F., de Visser, A., Ionov, S. G., Kulbachinskii, V. A., and Kytin, V. G. Magnetotransport in carbon foils fabricated from exfoliated graphite. *Physical Review B*, **1998**, 57, 8900–8906.

[19] Hargrove, J.; Shasikala, H. B. M.; Guerrido, L.; Ravi, N. and Wang, X.-Q. Band gap opening in methane Intercalated Graphene. *Nanoscale*, **2012**, 4, 4443.

[20] Schrodinger, E. Quantisierung als Eigenwertproblem (Erste Mitteilung). *Ann.der Physik*, **1926**, 79, 361.

[21] Fermi E., Eine statistische Methode zur Bestimmung einiger Eigenschaften des Atoms und ihre Anwendung auf die Theorie des periodischen Systems der Elemente. *Z. Phys.*, **1928**, 48, 73-79.

[22] Thomas, L. The calculation of atomic fields. *Proc. Cambridge Philos.*, **1927**, 23, 542-548.

[23] Balazs, N. Formation of Stable Molecules within the Statistical Theory of Atoms. *Phys. Rev.*, **1967**, 156, 42-47.

[24] Lieb, E. and Simon, B. Thomas-Fermi Theory Revisited. *Phys. Rev. Lett.*, **1973**, 31, 681-683.

[25] Teller, E. On the Stability Of Molecules In the Thomas-Fermi Theory. *Rev. Mod. Phys.*, **1962**, 34, 627.

[26] Jones, R.O. and Gunnarsson, O. The density functional formalism, its applications and prospects, *Rev. Mod. Phys.*, **1989**, 61, 689-746.

[27] Fock, V. Näherungsmethode zur Lösung des quantenmechanischen Mehrkörperproblems. *Z. Phys.*, **1930**, 61, 126.

[28] Pines, D. Electronic Interaction in Metals. *Solid State Physics*, **1955**, 1, 367.

[29] Hohenberg, P. and Kohn, W. Inhomogeneous Electron Gas. *Phys. Rev.*, **1964**, 136, B864-B871.

[30] Delley, B. An all-electron numerical method for solving the local density functional for polyatomic molecules. *J. Chem, Phys.*, **1990**, 92, 508.

[31] Kohn, W.; Becke. A. and Parr, R. Density Functional Theory of Electronic Structure. *J. Phys. Chem.*, **1996**, 100, 12974-12980.

[32] Eschrig, H. The Essentials of Density Functional Theory and the Full-Potential Local-Orbital Approach. *Lectures notes in Physics*, **2004**, 642, 7-21.

[33] Kohn, W. and Sham, L. J. Self-consistent equations including exchange and correlation effects. *Phys. Rev.*, **1965**, 140, A1133-A1138.

[34] Hafner J.; Wolverton C. and Ceder G. Toward computational materials design: the impact of density functional theory on materials research. *MRS Bulletin*, **2006**, 31, 659-668.

[35] Heinonen, O.; Lubin, M. and Johnson M. Ensemble Density Functional Theory of the Fractional Quantum Hall Effect. *Phys. Rev. Lett.*, **1995**, 75, 4110-4113.

[36] Kohn, W. Nobel Lecture: Electronic structure of matter – wave functions and density functionals. *Rev. Mod. Phys.*, **1999**, 71, 1253-1266.

[37] Perdew, J. and Zunger, A. Self-interaction correction to density-functional approximations for many-electron systems. *Phys. Rev. B*, **1981**, 23, 5048-5079.

[38] Vosko, S.; Wilk, L. and Nusair M. Accurate spin-dependent electron liquid correlation energies for local spin density calculations: a critical analysis. *Can. J. Phys.*, **1980**, 58, 1200-1211.

[39] Krasheninnikov A., Computational Methods for Material Science. 2000, University of Helsinki.

[40] Dresselhaus, M.S. and Dresselhaus, G. Intercalation compounds of graphite. *Advances in Physics*, **1981**, 30, 139–326.

[41] Kumar, A.; Reddy, A.L.M.; Mukherjee, A.; Dubey, M.; Zhan, X.; Singh, N.; Ci, L.; Billups, W.E.; Nagurny, J.; Mital, G. and Ajayan, P.M. Direct synthesis of lithium-

intercalated graphene for electrochemical energy storage application. *ACS Nano*, **2011**, 5, 4345–4349.

[42] Nathaniel, J. and Wang, X.-Q. Tunable electron and hole doping in FeCl3 intercalated graphene. *Applied Physics Letters*, **2012**, 100, 213112– 213113.

[43] Hiranandani, D.; Salimath, A.; Bishnoi, B.; Nandal, V.; Akram, M.W.; Jayanthi, A.; Yada, M.K. and Ghosh, B. Magnonscattering in single and bilayer graphene intercalates. *Journal of Applied Physics*, **2012**, 112, 114308–114309.

[44] Huang, Q. S.; Chen, X. L.; Lin, J. J.; Li, K.; Jia, Y.P.; Liu, J.; Guo, L.W.; Wang, W.J. and Wang, G. Preparation of Quasi-Free-Standing Graphene with a Super Large Interlayer Distance by Methane Intercalation. *J. Phys. Chem. C*, **2011**, 115, 20538-20545.

[45] Si, C.; Zhou, G.; Li, Y.C.; Wu, J. and Duan, W.H. Interface engineering of epitaxial graphene on SiC(0001) via fluorine intercalation: A first principles study. *Appl. Phys. Lett.*, **2012**, 100, 103105.

[46] Hsu, C.-H.; Lin, W.-H.; Ozolins, V. and Chuang, F.-C. Electronic structures of an epitaxial graphene monolayer on SiC(0001) after metal intercalation (metal=Al, Ag, Au, Pt, and Pd): A first-principles study. *Appl. Phys. Lett.*, **2012**, 100, 063115.

[47] Malik, S.; Vijayaraghavan, A.; Erni, R.; Ariga, K.; Khalakhan, I. and Hill, J.P. High purity graphene prepared by a chemical intercalation method. *Nanoscale*, **2010**, 2, 2139-2143.

[48] Boukhvalov, D.W. and Virojanadara, C. Penetration of alkali atoms throughout a graphene membrane theoretical modeling. *Nanoscale*, **2012**, 4, 1749.

[49] Deretzis, I. and La Magna, A. Role of covalent and metallic intercalation on the electronic properties of epitaxial graphene on SiC(0001). *Phys. Rev. B*, **2011**, 84, 235426.

[50] Aoki, M. and Amawashi, H. Dependence of band structures on stacking and field in layered graphene. *Solid State Communications*, **2007**, 142, 123–127.

[51] Guinea, F.; Neto, A.H.C. and Peres, N.M.R. Electronic states and landau levels in graphene stacks. *Phys. Rev. B*, **2006**, 73, 245426.

[52] Lu, C.L.; Chang, C.P.; Huang, Y.C.; Chen, R.B. and Lin, M.L. Influence of an electric field on the optical properties of few-layer graphene with AB stacking. *Phys. Rev. B*, **2006**, 73, 144427.

[53] Partoens, B. and Peeters, F. M. From graphene to graphite: Electronic structure around the K-point. *Phys. Rev. B*, **2006**, 74, 075404.

[54] Reina, A.; Jia, X.; Ho, J.; Nezich, D.; Son, H.; Bulovic, V.; Dresselhaus, M.S. and Kong, J. Large Area, Few-Layer Graphene Films on Arbitrary Substrates by Chemical Vapor Deposition. *Nano Lett.,* **2009**, 9, 30-35.

[55] $DMol_3$, Accelrys Software Inc., San Diego, CA, 2011.

[56] Schwierz, F. Graphene transistors. *Nature Nanotechnology,* **2010**, 5, 487-496.

[57] Samarakoon, D.K.; Chen, Z.; Nicolas, C. and Wang, X.-Q. Structural and Electronic Properties of Fluorograhene. *Small*, **2011**, 7, 965-969.

[58] Partoens, B. and Peeters, F.M. From graphene to graphite: Electronic structure around the K point. *Phys. Rev. B,* **2006**, 74, 075404.

[59] Latil, S. and Henrard, L. Charge Carriers in Few-Layer Graphene Films. *Phys. Rev. Lett.*, **2006**, 97, 036803.

[60] Grueneis, A.; Attaccalite, C.; Wirtz, L.; Shiozawa, H.; Saito, R.; Pichler, T. and Rubio, A. Tight-binding description of the quasiparticle dispersion of graphite and few-layer graphene. *Phys. Rev. B,* **2008**, 78, 205425.

[61] Avetisyan, A.A.; Partoens, B. and Peeters, F.M. Stacking order dependent electric field tuning of the band gap in graphene multilayers. *Phys. Rev. B,* **2010**, 81, 115432.

[62] Zhang, Y.; Tang, T.-T.; Girit, C.; Hao, Z.; Martin, M.C.; Zettl, A.; Crommie, M.F.; Shen, Y.R. and Wang, F. Direct observation of a widely tunable bandgap in bilayer graphene. *Nature,* 2009, 459, 820-823.

[63] Craciun, M.F; Russo, S.; Yamamoto, M.; Oostinga, J.B.; Morpurgo, A.F. and Thrucha, S. Trilayer graphene is a semimetal with a gate-tunable band overlap. *Nat. Nanotechnol.*, **2009**, 4, 383-388.

[64] Wang, H.M.; Wu, Y.H.; Ni, Z.H. and Shen, Z.X. Electronic transport and layer engineering in multilayer graphene structures. *Appl. Phys. Lett.*, **2008**, 92, 053504.

[65] Sahu, B.; Min, H.; MacDonald, H.A. and Banerjee, S.K. Energy gap, magnetism, and electric-field effects in bilayer graphene nanoribbons. *Phys. Rev. B,* **2008**, 78, 045404.

[66] Zhang, Z.; Chen, C.; Zeng, X.C. and Guo, W. Tuning the magnetic and electronic properties of bilayer graphene nanoribbons on Si(001) by bias voltage. *Phys. Rev. B,* **2010**, 81, 155428.

[67] Sahu, B.; Min , H. and Banerjee, S.K. Effects of edge magnetism and external electric field on energy gaps in multilayer graphene nanoribbons. *Phys. Rev. B,* **2010**, 82, 115426.

[68] Samarakoon, D.K. and Wang, X.-Q. Tunable band gap in hydrogenated bilayer graphene. *ACS Nano,* **2010**, 4, 4126-4130.

[69] Partoens, B. and Peeters, F.M. Normal and Dirac fermions in graphene multilayer's: Tight-binding description of the electronic structure. *Phys. Rev. B,* **2007**, 75, 193402.

[70] Williams, M.D.; Samarakoon, D.K; Hess, D.W. and Wang, X.-Q. Tunable bands in biased multilayer expitaxial graphene. *Nanoscale*, **2012**, 4, 2962-2967.

[71] Mele, E.J. Commensuration and interlayer coherence in twisted bilayer graphene. *Phys. Rev. B,* **2010**, 81, 161405.

[72] Kindermann, M. and Mele, E.J. Landau Quantization in Twisted Bilayer Graphenes: the Dirac Comb. *Phys. Rev. B,* **2011**, 84, 161406(R).

[73] Perdew, J.; Burke, K. and Ernzerhof, M. Generalized Gradient Approximation Made Simpple. *Phys. Rev. Lett.*, **1996**, 77, 3865 -3868.

[74] de Heer, W.A.; Berger, C.; Ruan, M.; Sprinkle, M.; Li, X.; Hu, Y.; Zhang, B.; Hankinson, J. and Conrad, E.H. Large area structured epitaxial graphene produced by confinement controlled sublimation of silicon carbide. *Proc. Natl. Acad. Sci. USA,* **2011**, 108, 16900.

[75] Plachinda P.; Evans, D.R. and Solanki, R. Electron of properties of metal-arene functionalized graphene. *J. Chem. Phys.*, **2011**, 135, 044103.

[76] Suggs, K.; Reuven, D. and Wang X.-Q. Electronic properties of cycloaddition functionalized graphene. *J. Phys. Chem. C*, **2011**, 115, 3313-3317.

[77] Jorio, A.; Dresselhaus, M.S.; Saito, R. and Dresselhaus, G. Raman Spectroscopy in Graphene Related Systems. John Wiley & Sons, 2011.

[78] Boukhvalov, D.W and Katsnelson, M.I. Chemical functionalization of graphene. Journal of Physics, **2009**, 21, 334205.

[79] Elias, D.C.; Nair, R.R.; Mohiuddin, T.M.G.; Morozov, S.V.; Blake, P.; Halsall, M.P.; Ferrari, A.C; Boukhvalov, D.W.; Katsnelson, M.I.; Geim, A.K. and Novoselov, K.S. Control of Graphene's Properties by Reversible Hydrogenation: Evidence for Graphane. *Science*, **2009**, 323, 610-613.

[80] Lebegue, S.; Klintenberg, M.I.; Eriksson, O. and Katsnelson, M.I. Accurate electronic band gap of pure and functionalized graphane from GW calculations. *Phys. Rev. B*, **2009**, 79, 245117.

[81] Gao, H.; Wang, L.; Zhao, J.; Ding, F. and Lu, J. Band Gap Tuning of Hydrogenated Graphene: H Coverage and Configuration Dependence. *J. Phys. Chem. C*, **2011**, 115, 3236-3242.

[82] Leenaerts, O.; Peelaers, H.; Hernandez-Nieves, A.D.; Partoens, B. and Peeters, F.M. First-principles investigation of graphene fluoride and graphane. *Phys. Rev. B*, **2010**, 82, 195436.

[83] Robinson, J.T.; Burgess, J.S.; Junkermeier, C.E.; Badescu, S.C.; Reinecke, T.L.; Perkins, F.K.; Zalalutdniov, M.K.; Baldwin, J.W.; Culbertson, J.C.; Sheehan, P.E.; Snow, E.S. Properties of fluorinated graphene films. *Nano Lett.*, **2010**, 10, 3001-3005.

[84] Yang, M.; Zhou, L.; Wang, J.; Liu, Z. and Liu, Z. Evolutionary Chlorination of Graphene: From Charge -Transfer Complex to Covalent Bonding and Nonbonding. *J. Phys. Chem. C*, **2012**, 116, 844-850.

[85] Chen, W.; Chen, S.; Qi, D.C.; Gao, X.Y. and Wee, A.T.S. Surface Transfer p-Type Doping of Epitaxial Graphene. *J. Am. Chem.*, **2007**, 129, 10418-10422.

[86] Wang, X.; Li, X.; Zhang, L.; Yoon, Y.; Weber, P.K.; Wang, H.; Guo, J. and Dai, H. N-Doping of Graphene Through Electrothermal Reactions with Ammonia. *Science*, **2009**, 324, 768-771.

[87] Calzolari, A.; Marzari, N.; Souza, I. and Buongiorno Nardelli, M. Ab initio transport properties of nanostructures from maximally localized Wannier functions. *Phys. Rev. B*, **2004**, 69, 035108.

[88] Kanungo, M.; Lu, H.; Malliaras, G.G.; Blanchet, G.B. Suppression of metallic conductivity of single-walled carbon nanotubes by cycloaddition reactions. *Science*, **2009**, 323, 234-237.

[89] Veloso, M.V.; Filho, A.G.S.; Filho, J.M.; Fagan, S.B.; Mota, R. Ab initio study of covalently functionalized carbon nanotubes. *Chem. Phys. Lett.*, **2006**, 430, 71-74.

[90] Park, H.; Zhao, J. and Lu, J.P. Distinct properties of SWNTs with monovalent side-wall additions. *Nanotechnology*, **2005**, 16, 635-638.